

7.6 Remote Sensing Vegetation Recovery after Forest Fires using Energy Balance Algorithm

J. Wang*, T. W. Sammis, C. A. Meier, L. J. Simmons, D. R. Miller, and D. J. Bathke
Agronomy and Horticulture Department, New Mexico State Univ., Las Cruces, New Mexico

Presented at the Sixth Symposium on Fire and Forest Meteorology Sponsored by American Meteorological Society

**Radisson Hotel Canmore, AB, Canada
25–27 October, 2005**

1. ABSTRACT

Information on the temporal and spatial dynamics of post-fire vegetation recovery and water use is essential for establishing post-fire vegetation management and for evaluating reforestation programs to reduce the risk of landslides and soil erosion after forest fires. Remote sensing techniques have been increasingly used as a convenient tool for monitoring vegetation cover and water stress. Commonly used techniques include spectral analysis, such as the Normalized Vegetation Index (NDVI). However, the accuracy of the spectral analysis can be significantly affected by the illumination geometry and the optical properties of the soil background. Furthermore, spectral analysis can not estimate absolute water use of plants. Alternatively, satellite derived estimates of spatial evapotranspiration (ET) computed using a Surface Energy Balance Algorithm for Land (SEBAL©) provide a more accurate means for monitoring vegetation changes and water consumption. In this paper, we use a modified SEBAL© to estimate and compare ET at the burned and unburned areas at Los Alamos, New Mexico where the Cerro Grande Fire burned 43,000-acre area on May 8-15, 2000. By comparing our results to point measurements, we demonstrate that this method is appropriate for estimating spatial and temporal ET and vegetation recovery after forest fires.

* *Corresponding author address:* Junming Wang, New Mexico State Univ., Agronomy & Horticulture Dept., MSC3Q, BOX 30003, Las Cruces, NM, 88003-8003; e-mail: junmingwang@yahoo.com

2. INTRODUCTION

The average number of annual forest fires (1991-2001) in the United States, both small and large, was 102,131 which resulted in an average burned area of 1,631,560 ha (UN, 2002). Differences in fire patterns, plant height, species composition, and topography result in highly variable vegetation damage from forest fires (Díaz-Delgado et al., 2003). Forest fires also have indirect impacts on vegetation. For example, post-fire vegetation cover can be decreased due to erosion and substrate loss (Alcañiz et al., 1996). Additionally, different plant strategies for regeneration after fire (i.e., massive seed production, replanting, etc.) can drive differences in the vegetation recovery rate. Topography (i.e., elevation, aspect, and slope) in the burned area also has a considerable effect on both plant recovery and vegetation loss due to fire damage (Díaz-Delgado et al., 2003)

Estimates of vegetation recovery and water use after forest fires can aid forest management and provide a means of evaluating remediation work. Though point measurements (sampling different locations) of forest vegetation cover and water use are useful, they are too time-consuming and costly to apply on large-scale areas such as forests (Buckley et al., 2003; Miller et al., 2005; Sammis et al., 2002; Sammis et al., 2004). Alternatively, remote sensing has proven to be a convenient and economically feasible tool for determining fire severity impact on vegetation cover (Caetano et al., 1994; Caetano et al., 1996; White et al., 1996) and for monitoring plant regeneration after fire (Díaz-Delgado and Pons, 2001). In addition to their spatial resolution potential, satellite images can also be used to produce a time series of the vegetation cover to

detect and monitor land cover changes. Moreover, advances in this subject can aid in defining new post-fire management criteria in burned areas under different fire severity levels.

To detect relative fire damage, vegetation cover and water stress, researchers usually use spectral analysis such as Normalized Difference Vegetation Index (NDVI) which reflects the leaf greenness (Díaz-Delgado and Pons, 2001). Although this method has received several good reviews (Boyd and Danson, 2005; Treitz and Howarth, 1999; Ustin et al., 2004; Wulder, 1998; Wulder et al., 2004), its accuracy can be significantly affected by illumination geometry, and optical properties of the soil background.

As an alternate means of detecting vegetation changes, several different methods have been developed to estimate spatial ET for level crop fields based on satellite data. ET consists of plant transpiration and ground water evaporation. When the soil surface is dry, ET results only from plant transpiration. Thus, the percent vegetation cover can be determined by dividing the ET at the area of interest by the ET of the full plant cover area. Since ET estimates from satellite data are not sensitive to sun illumination and optical properties of the soil background, it can provide a more accurate estimate of changes in vegetation.

Most ET models use thermal infrared data (TIR) to obtain the surface temperature (T_s) and then calculate ET as the difference between the surface and air temperature (dT). However, it is difficult to obtain the required precision for surface temperature from satellite measurements and errors in surface temperature determination cause significant errors in ET calculations. The SEBAL© averts this problem by calibrating apparent radiative temperature to sensible heat flux (H). This algorithm is based on the assumption that the surface-to-air temperature difference is linearly related to the apparent radiative temperature. Consequently, with knowledge of the aerodynamic resistance and height of the canopy cover in each pixel, one can compute H and ET (Bastiaanssen et al., 1998; Bastiaanssen et al., 2005). Thus, SEBAL© approach is an attractive approach for

operational applications of ET calculation (Courault et al., 2003). SEBAL© technology has been successfully used in 40 applications in 25 countries with accuracies of 85% on a daily basis and 95% on a seasonal basis (Bastiaanssen et al., 2005). Though SEBAL© is widely used for level crop fields, little work has been done for forests on sloping terrain.

The accuracy of ET estimates determined from remote sensing and ET models can be assessed from independently collected ground measurements. Because eddy-covariance methods (EC) provide one of the most reliable measurements of evaporation fluxes, EC is often used to validate ET models. EC may be implemented with measurement of both latent heat and sensible heat fluxes, using sonic anemometers and fast-response infrared gas analyzers such as the LI-COR 7500 (SEC system, Miller et al., 2005).

In this study, we modified SEBAL© and developed Satellite ET model (SET) to evaluate forest ET at burned and unburned areas to infer changes in the vegetation cover. The model is validated using ET and vegetation cover data after the Cerro Grande Fire at Los Alamos (May 8-15, 2000).

3. MATERIALS AND METHODS

Model

A SET model written in the C++ program language was developed and validated at New Mexico State University. This model estimates ET and percent vegetation cover at a 90 m \times 90 m resolution using ASTER and local weather data. The ASTER data is available online from the NASA Earth Observing System Data Gateway (<http://redhook.gsfc.nasa.gov/~imswww/pub/imswelco.me/>). The weather data was obtained from a nearby remote automated weather station (Mountainair RAWS) processed by the New Mexico Climate Center.

The general flowchart of the SET model is shown in Figure 1. First, the model inputs ASTER satellite data and local weather data. Then, it calculates the NDVI, the soil heat flux (G) and the sensible heat (H) flux. Finally, the model outputs the spatial ET (mm/hr) and percent vegetation cover according to the energy

budget equation.

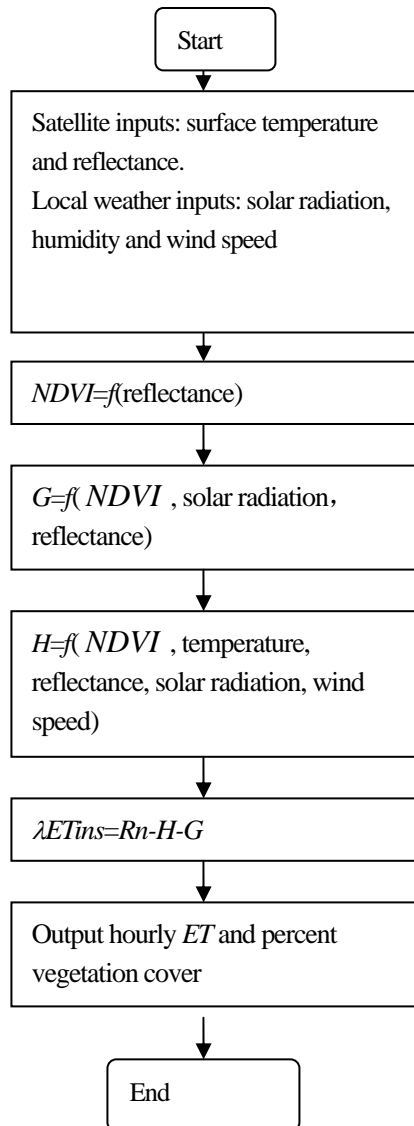


Figure 1. The general flowchart of the SET model.

At each pixel on the output ET map, the percent vegetation cover is calculated by dividing the ET value at the area of interest by the average ET at the unburned area.

Inputs

Model inputs include wind speed, humidity and solar radiation data from the local weather station and satellite data products from ASTER including ground surface reflectance and temperature. The reflectance has a resolution of 15 m × 15 m for

bands 1 to 3 (Visible and Near-infrared bands) and 30 m × 30 m for bands 4 to 9 (Shortwave Infrared bands). Because the temperature data has a resolution of 90 m × 90 m, the reflectance data were averaged over 90 m × 90 m to fit the resolution of the temperature data. This model does not calculate ground surface temperature and reflectance; the data products are obtained from the ASTER website directly. This simplified the model complexity, which in turn reduces the program work and time, and guarantees the quality of the data products.

Outputs

The spatial ET (mm/hr) and percent vegetation cover are output from the model at a resolution of 90 m × 90 m.

Theory

The model method uses the energy budget equation to calculate the instant latent heat loss (λET_{ins}) in W/m^2 for each pixel at the time of the satellite overflight. Thus, the instant latent heat loss is given as

$$\lambda ET_{ins} = R_n - G - H \quad (1)$$

where R_n is net solar radiation (W/m^2), G is soil heat flux into the soil (W/m^2), and H is the sensible heat flux into the air (W/m^2).

In equation (1), R_n is calculated as the difference between R_{ns} , the local net short-wave radiation, and R_{nl} , the local net long-wave radiation (Walter et al., 2002), such that

$$R_n = R_{ns} - R_{nl} \quad (2)$$

Here,

$$R_{ns} = (1 - \alpha) R_s \quad (3)$$

where α is surface albedo and R_s is incoming solar radiation measured at the local weather station in (W/m^2).

In (3), α is calculated using the following equation given by Liang (2000), which uses ASTER surface reflectance data:

$$\alpha = 0.484\alpha_1 + 0.335\alpha_3 - 0.324\alpha_5 + 0.551\alpha_6 + 0.305\alpha_8 - 0.367\alpha_9 - 0.0015 \quad (4)$$

where α_i is the reflectance for ASTER data band i.

Rnl is calculated using the following equation given by (Walter et al., 2002):

$$Rnl = 277.8\sigma T_s^4 (0.34 - 0.14\sqrt{e_a}) \quad (5)$$

where T_s =mean absolute surface temperature (K), which is obtained from the satellite data, and σ =Stefan-Boltzmann constant (2.042×10^{-10} MJ/K⁴/m²/hr), and e_a is the actual vapor pressure (kPa) such that

$$e_a = \frac{RH}{100} e_s(T_a). \quad (6)$$

In equation (6), $e_s(T_a)$ is saturation vapor pressure (kPa) given as

$$e_s(T_a) = 0.6108 \exp\left(\frac{17.27T_a}{T_a + 237.3}\right) \quad (7)$$

and T_a is air temperature (°C) defined as

$$T_a = T_s - dT - 273 \quad (8)$$

where dT is the difference between surface temperature and air temperature (K) as shown in equation (16).

From Equation (1), the heat flux into the soil, G , can be represented by

$$G = G / Rn \times Rn. \quad (9)$$

According to Bastiaanssen et al., (1998),

$$G / Rn = T_s(0.0032 + 0.0062\alpha)(1 - NDVI^4) \quad (10)$$

The NDVI is calculated using the reflectance data, α_3 and α_2 , from bands 3 and 2, respectively.

$$NDVI = \frac{\alpha_3 - \alpha_2}{\alpha_3 + \alpha_2} \quad (11)$$

For the calculation of the sensible heat flux, H , two pixels are chosen in the satellite data. One pixel is a wet pixel that represents a well-irrigated field having the surface temperature close to air temperature. The second pixel is a dry field where λET_{ins} is assumed to be 0. The two pixels can then be used to tie the calculations for all other pixels between these two points. At the dry pixel, we assume $\lambda ET_{ins} = 0$. Then according to equation (1),

$$H = Rn - G \quad (12)$$

The sensible heat flux, H , can also be represented by

$$H = \frac{\rho \times c_p \times dT}{r_{ah}} \quad (13)$$

where ρ is the air density (mol/m³), c_p is the specific heat of air (29.3 J/mol/ °C), dT is the near surface temperature difference (K), and r_{ah} is the aerodynamic resistance to heat transport (s/m) given as

$$r_{ah} = \frac{\ln\left(\frac{z_2}{z_1}\right)}{u^* k} \quad (14)$$

In (14), z_1 is a height just above the zero plane displacement height of the plant canopy (set to 0.1 m for each pixel) and z_2 is the reference height just above the plant canopy (set to 2 m for each pixel), u^* is the friction velocity (m/s), and k is the von Karman constant (0.4).

The friction velocity, u^* , can be calculated as

$$u^* = \frac{u(z)k}{\ln\left(\frac{z-d}{z_m}\right)} \quad (15)$$

where $u(z)$ is the wind speed at height of z , d (m) is the zero displacement height ($d=0.65h$), h is the plant height (m), and z_m is the roughness length (m, $z_m=0.1h$) (Campbell and Norman, 1998). Using equations (12-15) and the input data, dT at the dry spot (dT_{dry}) can be calculated. At the wet spot, we assume $H=0$ and $dT_{wet}=0$. Because the surface temperatures at the dry and wet spots (T_{dry} and T_{wet} , K) are also known, we can form the following linear equation for each pixel:

$$dT = \left(\frac{dT_{dry} - dT_{wet}}{T_{dry} - T_{wet}} \right) \times T_s - \left(\frac{dT_{dry} - dT_{wet}}{T_{dry} - T_{wet}} \right) \times T_{swet} \quad (16)$$

Then, according to equation (16), H at each pixel can be calculated by substituting values into equations (13-15). For these calculations, we assume that at 200 m the wind speed is the same for each pixel. First, the wind speed at 200 m is calculated for the weather station. Then u^* is solved for each pixel using equation (15). The parameter d in equation (15) is negligible when $z=200$ m; therefore it is set to 0. The z_m for each pixel is calculated using a regression equation and known values of z_m and NDVI at three sample pixel locations. For example, if we know that trees have $z_m=1.2$ m and NDVI=0.57, that grasses have $z_m=0.07$ m and NDVI =0.42, and that bare soil has $z_m=0.003$ m and NDVI =0.18, we can obtain a regression equation for z_m (Figure 2).

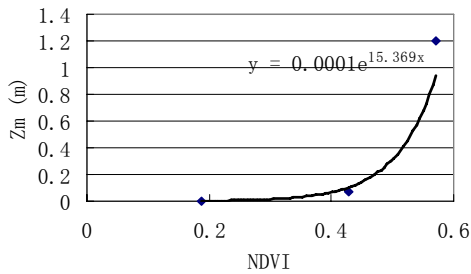


Figure 2. Example regression equation for determining z_m from NDVI.

Because atmospheric stability may have effects on H , an atmospheric correction is calculated (Figure 3). First the u^* and wind speed at 200 m is determined for the local weather station. Then z_m , u^* and dT are computed for each pixel and r_{ah} and H

without the atmospheric correction are obtained. Additionally, the stability parameter or Obukhov length, L (m), is calculated. Finally, u^* , r_{ah} , and H are corrected. Updated values for L , u^* , r_{ah} , and H are computed during successive iterations until H converges (i.e., does not change more than 10%). The atmospheric correction equations (Campbell and Norman, 1998; Stull, 2001) are shown below in equations (17-25). The stability parameter, or Obukhov length, L , is defined as

$$L = -\frac{u^{*3} T_s}{kgH} \quad (17)$$

where u^* is the friction velocity, T_s is the surface temperature, k is the von Karman constant, g is the acceleration due to gravity, and H is the sensible heat flux. When $L < 0$, H is positive and heat is transferred from the ground surface to the air under unstable conditions. Conversely, when $L > 0$, H is negative and heat is transferred from the air to the ground surface under stable condition. Finally when $L=0$, no heat flux occurs and conditions are neutral. Because the satellite overflight occurred at local noon time, we assume that the atmosphere was unstable. Therefore, when $L > 0$ (stable) occurred, we forced $L=0$ (neutral).

The correction factor for atmospheric momentum transport, ϕ for stable and neutral conditions is

$$\phi\left(\frac{z}{L}\right) = 0 \quad \text{for } L=0 \quad (18)$$

$$\phi\left(\frac{z}{L}\right) = -2\ln\left(\frac{1+\beta}{2}\right) - \ln\left(\frac{1+\beta^2}{2}\right) + 2\tan^{-1}(\beta) - \frac{\pi}{2} \quad \text{for } L < 0 \quad (19)$$

In (19), the parameter β is

$$\beta = [1 - 15(z - d)/L]^{0.25} \quad (20)$$

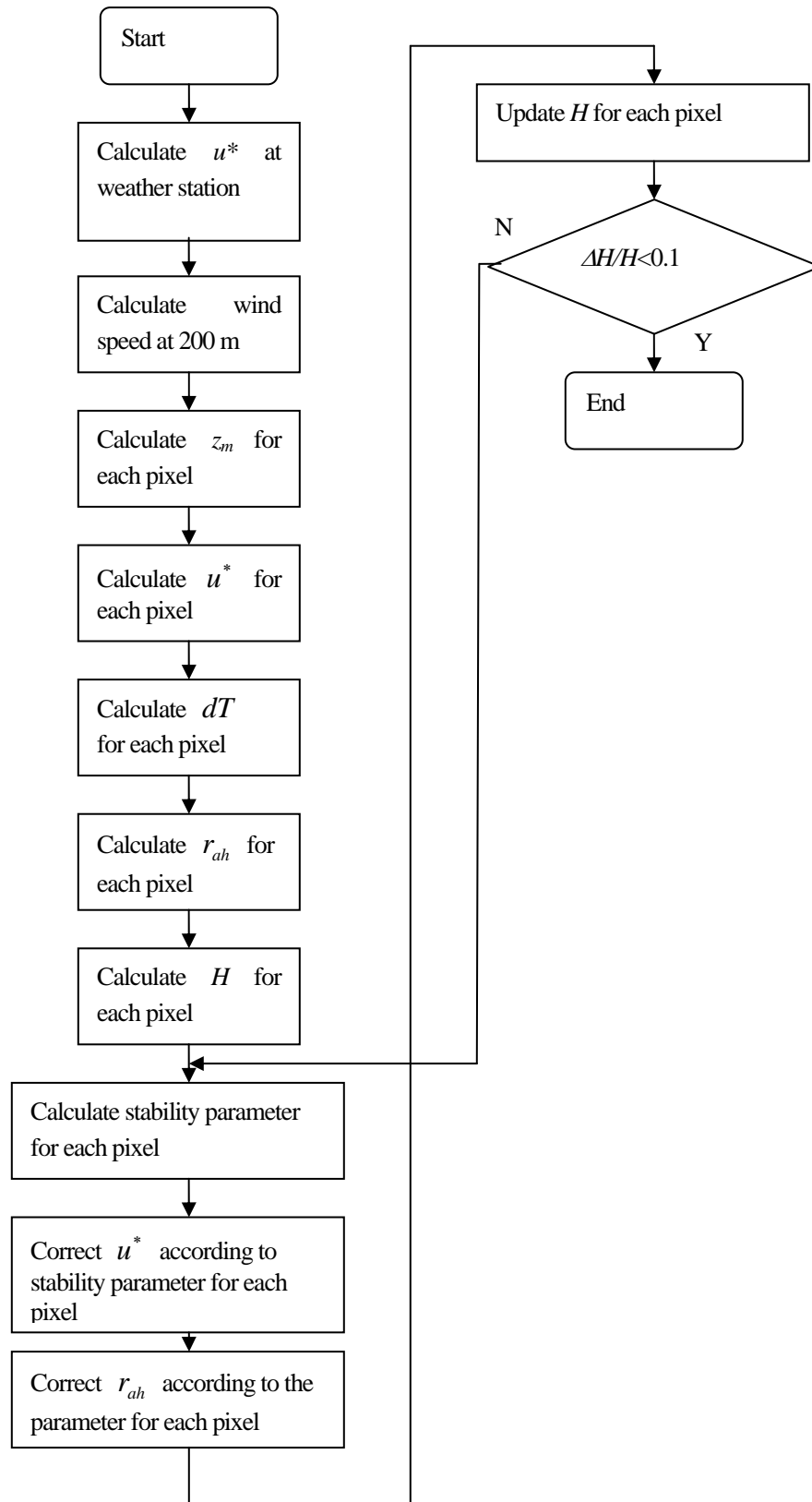


Figure 3. Atmospheric correction for H.

With the momentum correction factor, u^* in equation (15) can now be written as

$$u^* = \frac{ku(z)}{\left[\ln\left(\frac{z-d}{z_m}\right) + \varphi\left(\frac{z}{L}\right) \right]} \quad (21)$$

If $z=200$ m, then d is negligible ($d=0$).

Lastly, the correction term for the heat transfer, ψ , is

$$\psi(z) = 2 \ln\left(\frac{1 + \beta_z^2}{2}\right) \quad \text{for } L < 0 \quad (22)$$

$$\psi(z) = 0 \quad \text{for } L = 0 \quad (23)$$

Using the heat transfer correction term in (23), r_{ah} in equation (14) becomes

$$r_{ah} = \frac{\ln\left(\frac{z_2}{z_1}\right) - \psi(z_2) + \psi(z_1)}{u^* k} \quad (24)$$

Once H is corrected for the atmospheric effects, λET_{ins} for each pixel can be calculated using equation (1) and the hourly ET (ET_{hourly}, mm/hr) can be calculated as follows:

$$ET_{hourly} = \frac{\lambda ET_{ins}}{\lambda ET_{rins}} ET_r, \text{ hourly} \quad (25)$$

where λET_r , hourly is the hourly ET for well-irrigated alfalfa, which can be obtained by the FAO Penman-Monteith equation, and λET_{ins} (W/m^2) is the instant λET for a well-irrigated alfalfa field, which is calculated using equations 1-9 ($\alpha=0.23$, $G/R_n=0.04$, and $T_s=T_{swet}$).

The evaluation site and measurements

The model evaluation site was chosen at Los Alamos, NM (Figure 4) where the Cerro Grande Fire occurred on May 8-15, 2000. Two ET measurement towers set up by the Los Alamos

National Laboratory have been measuring 15-min latent heat fluxes at this location since the 1990s (Rishel et al., 2003). The TA-6 tower measures latent heat flux at 11.5 m using a folded-path optical infrared hygrometer (IR-2000, Ophir Corporation, Littleton, CO) and a 3-D sonic anemometer (SWS-211/3Sx, Applied Technologies, Inc, Longmont, Co). It is located on the Pajarito Plateau (N35.8614/W106.3196) in the burned area. The TA-54 tower also measures latent heat flux at 11.5 m using the same instruments as at TA-, but it is located in a clearing in piñon/juniper woodland at the eastern edge of Mesita del Buey (N35.8258/W106.2233). The latent heat data was processed to hourly ET (mm/hr) and was corrected according to Miller et al. (2005). The TA-54 location has a similar elevation as that of the burned area. Additionally, the lake and rock areas at the study site were chosen as the wet and dry spots, respectively.

The ASTER data is available for June 10, 2000, approximately one month after the fire and again on September 23, 2003, about three years after the fire. Weather data available from the New Mexico Climate Center (<http://weather.nmsu.edu>) indicate that little rain occurred on the two ASTER overflight dates and within the preceding 10 days.

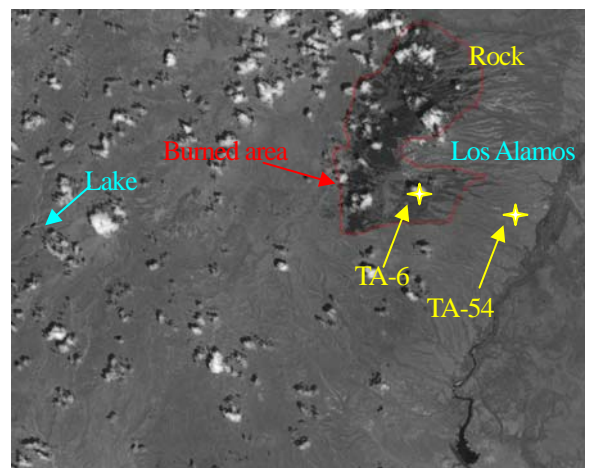


Figure 4. The Los Alamos study site (the ASTER band-3 radiance image)

Elevation and slope correction

The wet (lake) and dry (rock) spots have a similar elevation as the burned area. Consequently, we did not correct the elevation effects on ET calculation for the burned area. Because the satellite overflight at Los Alamos occurred at noon and the burned-area slope angle from the horizon is small, we assume that the slopes did not have significant effects on the incoming solar radiation and ET calculation. As such, the slope corrections in the ET calculation were not conducted.

ET observation and simulation comparison

The measured and simulated ET and the percent vegetation cover were compared by graph analysis to determine the applicability of the SET model. To represent the tower ET simulation, the average ET at 5 simulated points around the corresponding measurement tower was calculated. The percent vegetation cover data at TA-6 location was obtained from Buckley et al. (2003).

4. RESULTS AND DISCUSSION

The ET maps for the area of the Los Alamos fire in 2000 and 2003 are shown in Figure 5 and 6, respectively. The unburned area had an average ET of 0.8 mm/hr on June 10, 2000 and 0.5 mm/hr on September 23, 2003 whereas the severely burned area had an ET of 0 mm/hr in 2000 and 0-0.5 mm/hr in 2003. Accordingly, the severely burned area had 0% percent vegetation cover in June of 2000 and had later recovered to an average 47% percent vegetation cover by September of 2003.

Figure 7 shows the comparison of the ET model simulations vs. the actual measurements. This figure demonstrates that the model ET estimates correspond well with the point measurements. The observation and simulated values of percent vegetation cover for the summer of 2003 at the location of the TA-6 tower also are in close agreement (Figure 8). Figures 9 and 10 show the vegetation recovery from about 0% in 2000 to 25% in 2003 at TA-6. As these figures show, most of the recovered vegetation was grasses and shrubs.

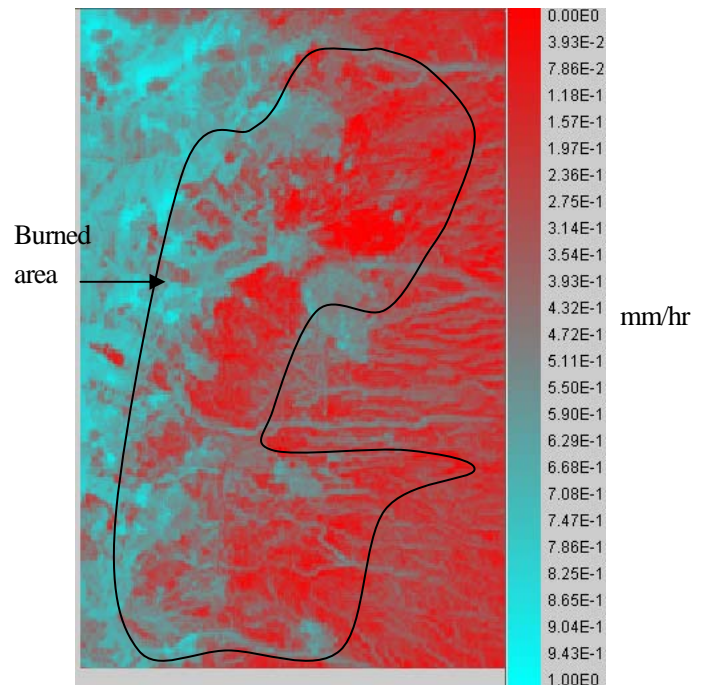


Figure 5. The ET map on June 10, 2000 (approximately one month after the fire). The false color was added using HDFView2.1. (<http://hdf.ncsa.uiuc.edu/hdf-java-html/hdfview/>).

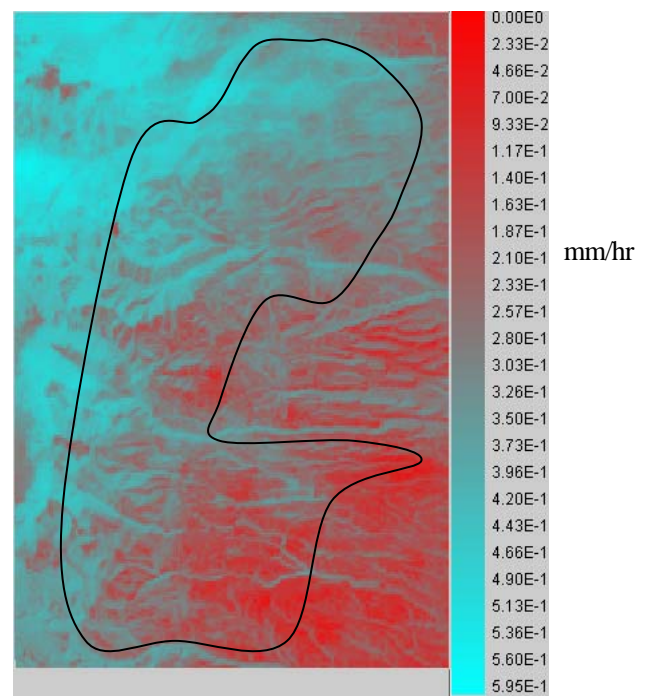


Figure 6. The ET map on September 23, 2003 (approximately three years after the fire).

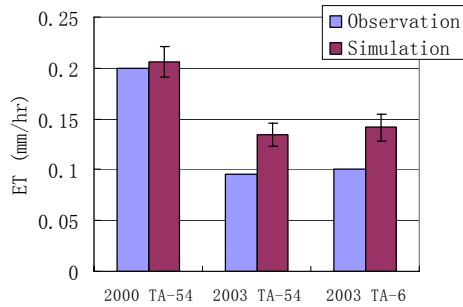


Figure 7. The comparison of simulated vs. observed ET for June 10, 2000 and September 23 2003 at the TA-54 tower and September 23, 2003 at the TA-6 tower. Vertical bars represent the standard deviations. Note: Cloudy conditions occurred at the TA-6 location on June 10, 2000.

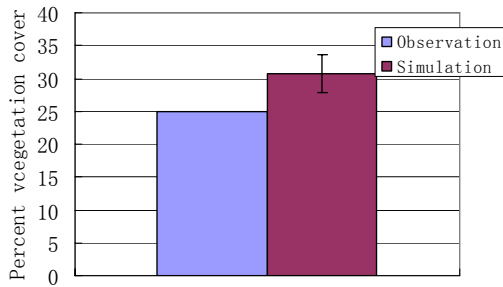


Figure 8. The simulated vs. observed percent vegetation cover at the TA-6 site in summer of 2003. The percent vegetation cover data was not available at TA-54.



Figure 10. The percent vegetation cover (25%) around TA-6 in July 2003 (Buckley et al., 2003).

5. CONCLUSION

The SET has been successfully used to provide accurate estimates of ET and vegetation recovery after the Cerro Grande Fire at Los Alamos. Thus, this model is an appropriate method for monitoring vegetation changes and for use in forest service management.

6. ACKNOWLEDGMENTS

The authors gratefully acknowledge financial support from the New Mexico State University's Agricultural Experiment Station. The authors thank Lyn McKinley at Department of Agricultural Communications and Dr. John Mexal at Agronomy and Horticulture Department in New Mexico State University for their great editing work.



Figure 9. The percent vegetation cover (0%) around TA-6 in July 2000 (Buckley et al., 2003).

7. REFERENCES

- Alcañiz, J.M., I. Serrasolsas, and R. Vallejo. 1996. Efectes dels incendis forestals sobre el sòl. In *Ecologia del Foc*, edited by J. Terradas (Barcelona: Proa), pp. 111–130.
- Bastiaanssen, W.G.M., M. Menenti, R.A. Feddes, and A.A.M. Holtslag. 1998. A remote sensing surface energy balance algorithm for land (SEBAL). 1. Formulation. *J. Hydrol.* 212/213:198-212.
- Bastiaanssen, W.G.M., E.J.M. Noordman, H. Pelgrum, G. Davids, B.P. Thoreson, and R.G. Allen. 2005. SEBAL model with remotely sensed data to improve water-resources management under actual field conditions. *Journal of irrigation and drainage engineering* 131:85-93.
- Boyd, D.S., and F.M. Danson. 2005. Satellite remote sensing of forest resources: three decades of research development. *Progress in Physical Geography* 29:1-26.
- Buckley, K.J., J.C. Walterscheid, S.R. Loftin, and G.A. Kuyumjian. 2003. Final Progress Report on Los Alamos National Laboratory Cerro Grande Fire Rehabilitation Activities. Los Alamos National Laboratory.
- Caetano, M., L. Mertes, L. Cadete, and J.M.C. Pereira. 1994. Using spectral mixture analysis for fire severity mapping. In 2nd Conference on Forest Fire Research, edited by L. A. Oliveira, D. X. Viegas, V. Varela and A. M. Raimundo (Coimbra: ADAI) II:667-677.
- Caetano, M., L. Mertes, L. Cadete, and J.M.C. Pereira. 1996. Assesment of AVHRR data for characterising burned areas and post-fire vegetation recovery. *EARSeL Advances in Remote Sensing* 4:124–134.
- Campbell, G.S., and J.M. Norman. 1998. An introduction to environmental biophysics Springer.
- Courault, D., B. Seguin, and A. Olioso. 2003. Review to estimate evapotranspiration from remote sensing data: some examples from the simplified relationship to the use of mesoscale atmospheric models. ICID workshop on remote sensing of ET for large regions, 17th September, 2003.
- Díaz-Delgado, R., and X. Pons. 2001. Spatial patterns of forest fires in Catalonia (NE Spain) along the period 1975–1995. Analysis of vegetation recovery after fire. *Forest Ecology and Management* 147: 67-74.
- Díaz-Delgado, R., F. Lloret, and X. Pons. 2003. Influence of fire severity on plant regeneration by means of remote sensing imagery. *Int. J. Remote Sensing* 24, 8:1751-1763.
- Miller, D.R., T.W. Sammis, L.J. Simmons, V.P. Gutschick, and J. Wang. 2005. Water use efficiency and net carbon assimilation in a mature irrigated pecan orchard. *ASAE Transaction*. In press.
- Rishel, J., S. Johnson, D. Holt, M. Coronado, and B. Olsen. 2003. Meteorological Monitoring at Los Alamos LA-UR-03-8097. Los Alamos National Laboratory, Los Alamos.
- Sammis, T.W., J.G. Mexal, and E.A. Herrera. 2002. Daily cycle of evapotranspiration from pecan trees. *Pecan South* 35:32-38.
- Sammis, T.W., J.G. Mexal, and D.R. Miller. 2004. Evapotranspiration of flood-irrigated pecans. *Agricultural water management*: 179-190.
- Stull, R.B. 2001. An introduction to boundary layer meteorology Kluwer Academic.
- Treitz, P.M., and P.J. Howarth. 1999. Hyperspectral remote sensing for estimating biophysical parameters of forest ecosystems. *Progress in Physical Geography* 23:359–390.
- UN. 2002. Forest Fire Statistics. *Timber Bulletin*. Food and Agriculture Organization of the United Nations. 4.
- Ustin, S.I., D.A. Roberts, J.A. Gamon, G.P. Asner, and R.O. Green. 2004. Using Imaging Spectroscopy to Study Ecosystem Processes and Properties. *BioScience*

54:523-534.

- Walter, I.A., R.G. Allen, R. Elliott, Itenfis, D.P. Brown, M.E. Jensen, B. Mecham, T.A. Howell, R. Snyder, S. Eching, T. Spofford, M. Hattendorf, D. Martin, R.H. Cuenca, and J.L. Wright. 2002. ASCE Standardized Reference Evapotranspiration Equation Environmental and Water Resources Institute of the American Society of Civil Engineers Standardization of Reference Evapotranspiration Task Committee.
- White, J.D., K.C. Ryan, C. Key, and S.W. Running. 1996. Remote sensing of forest fire severity and vegetation recovery. *International Journal of Wildland Fire* 6:125–136.
- Wulder, M. 1998. Optical remote-sensing techniques for the assessment of forest inventory and biophysical parameters. *Progress in Physical Geography* 22:449-476.
- Wulder, M.A., R.J. Hall, C.C. Coops, and S.E. Franklin. 2004. High Spatial Resolution Remotely Sensed Data for Ecosystem Characterization. *BioScience* 54:511-521.